Supporting Information for the manuscript:

Influence of the pyrazine substituent on the structure and magnetic properties of dicyanamide-bridged cobalt(II) complexes

Joanna Palion-Gazda,[a], Katarzyna Czerwińska, Barbara Machura,[a] Rafal Kruszynski,[b] Joan Cano*[c], Francesc Lloret[c] and Miguel Julve[c]*

[a]Department of Crystallography, Institute of Chemistry, University of Silesia, 9th Szkolna Street, 40006 Katowice, Poland

[b]Department of X-ray Crystallography and Crystal Chemistry, Institute of General and Ecological Chemistry, Lodz University of Technology,116 Żeromski St., 90-924 Łódź, Poland.

[c]Departament de Química Inorgànica/Instituto de Ciencia Molecular (ICMol), Universitat de València, C/ Catedrático José Beltrán 2, 46980 Paterna, València, Spain

Table of Contents

χ_M' *vs.* χ_M"·ϖ (green) and χ_M"/ϖ *vs.* χ_M"·ϖ (red) methods (bottom) which are described in the main text. The solid lines are the best-fit curves using Orbach-Orbach (dark), Orbach-direct (moderate) and Raman-direct (pale) approaches.	
21. χ_M' against either χ_M"/ϖ (top) or χ_M"·ϖ (middle) and χ_M"/ϖ *vs.* χ_M"·ϖ plots for **1** under an applied static field of H_{dc} = 2500 G in the temperature range 2.0–10.5 K.	Fig. S21
22. Arrhenius plots for **2** under an applied static field of H_{dc} = 1000 G obtained from temperature- (blue) and field- (red) dependences of χ_M" (top), and through the χ_M' *vs.* χ_M"/ϖ (blue), χ_M' *vs.* χ_M"·ϖ (green) and χ_M"/ϖ *vs.* χ_M"·ϖ (red) methods (bottom) which are described in the main text. The solid lines are the best-fit curves using Orbach-Orbach (dark), Orbach-direct (moderate) and Raman-direct (pale) approaches.	Fig. S22
23. Arrhenius plots for **2** under an applied static field of H_{dc} = 2000 G obtained from temperature- (blue) and field- (red) dependences of χ_M" (top), and through the χ_M' *vs.* χ_M"/ϖ (blue), χ_M' *vs.* χ_M"·ϖ (green) and χ_M"/ϖ *vs.* χ_M"·ϖ (red) methods (bottom) which are described in the main text. The solid lines are the best-fit curves using Orbach-Orbach (dark), Orbach-direct (moderate) and Raman-direct (pale) approaches.	Fig. S23
24. Crystal data and structure refinement of **1** and **2.**	Table S1
25. Selected bond lengths [Å] and angles [°] for **1**.	Table S2
26. Selected bond lengths [Å] and angles [°] for **2**.	Table S3
27. Hydrogen bonds and C–H···N type interactions in **1** and **2**[a]	Table S4
28. Short π···π interactions for **1** and **2**[a]	Table S5
29. C—X···Cg(J)(π-ring) (X = O, N) interactions for **2**[a]	Table S6
30. Energy of all calculated excited states and their contributions to the *D* and *E* values for the real geometries of Co1 in **1** and Co2 in **2** obtained from CASSCF/NEVPT2 calculations.	Table S7
31. Energy of all calculated excited states and their contributions to the *D* and *E* values for the real geometries of Co1 and Co1e in **2** obtained from CASSCF/NEVPT2 calculations.	Table S8
22. Energies of the low-lying Kramers doublets corresponding to the ground and first excited states, which should be related to those generated from the 1st order spin-orbit coupling, of the real geometries of Co1 in **1** and Co1, Co1e and Co2 in **2** obtained from CASSCF/NEVPT2 calculations.	Table S9
23. Selected ac magnetic data for **1** under H_{dc} = 1000 G	Table S10
24. Selected ac magnetic data for **1** under H_{dc} = 2500 G	Table S11
25. Selected ac magnetic data for **2** under H_{dc} = 1000 G	Table S12
26. Selected ac magnetic data for **2** under H_{dc} = 2000 G	Table S13
27. Selected ac magnetic data for **2** under H_{dc} = 3500 G	Table S14

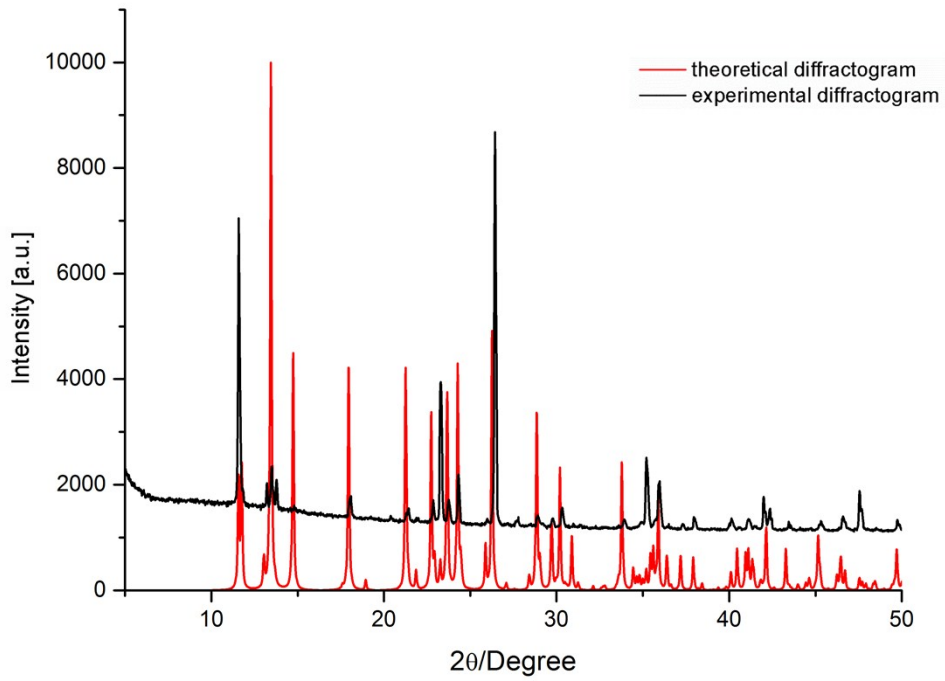

Figure S1. Powder XRPD pattern of **1** (experimental - black) and the simulation of its powder pattern from the crystal structure (red).

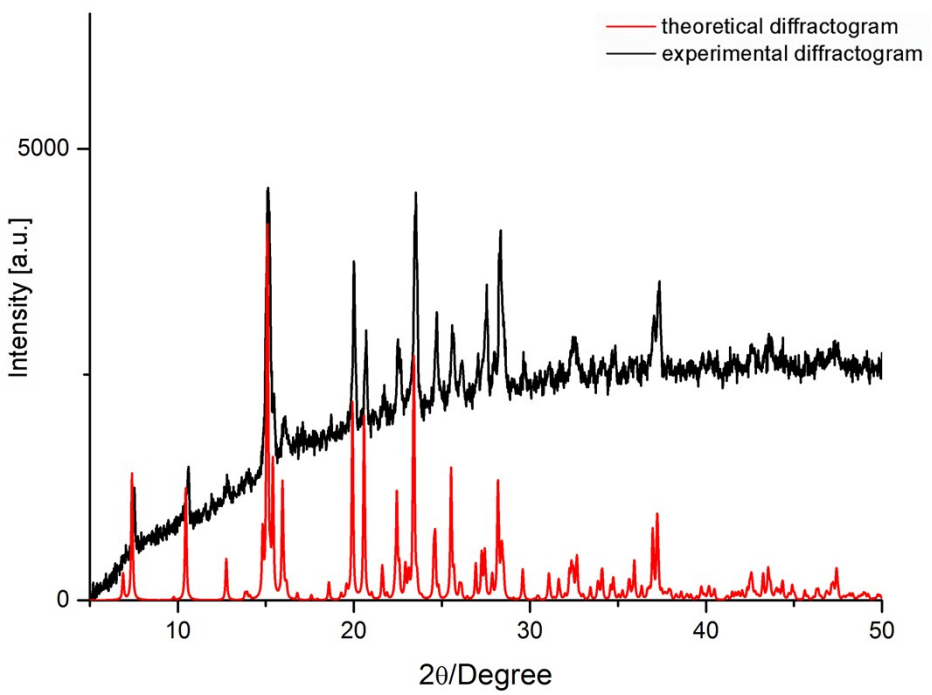

Figure S2. Powder XRPD pattern of **2** (experimental - black) and the simulation of its powder pattern from the crystal structure (red).

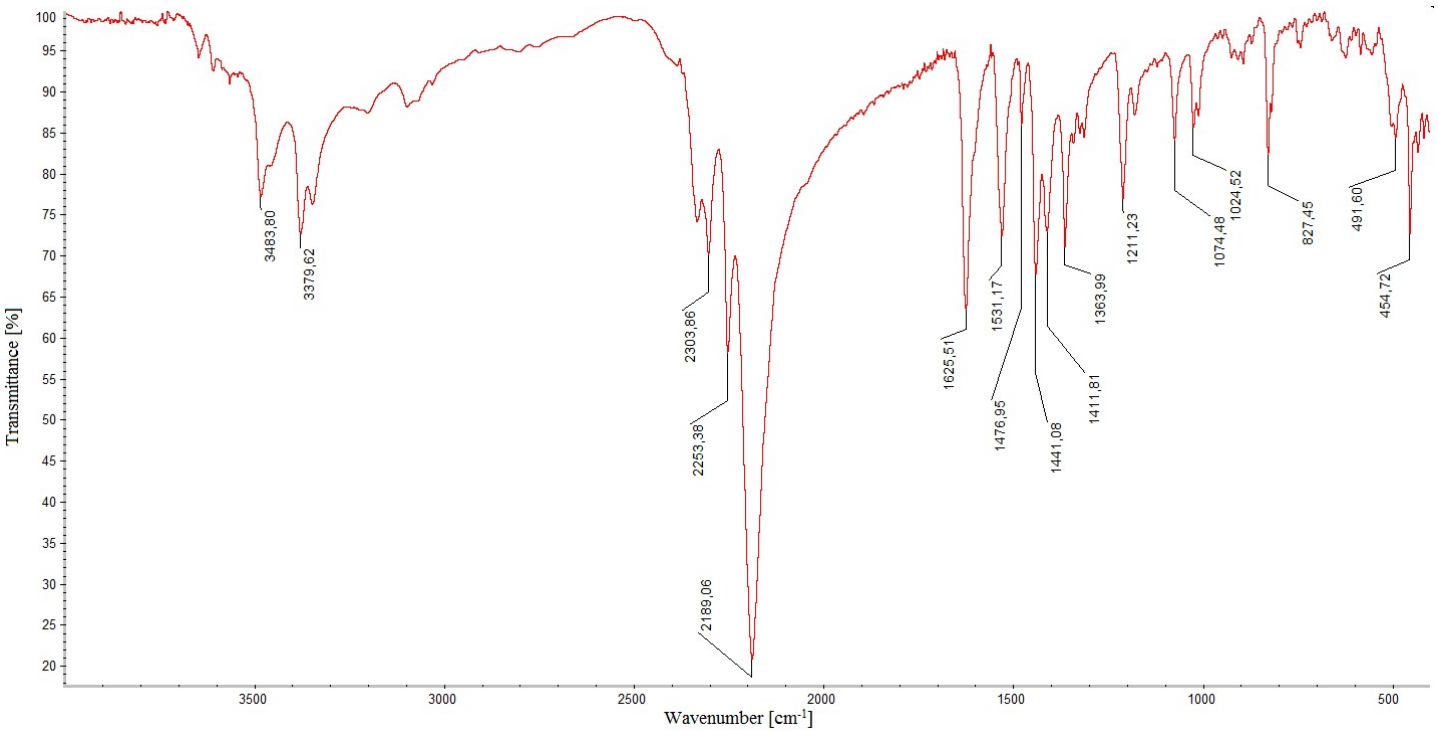

Figure S3. IR spectrum of **1**.

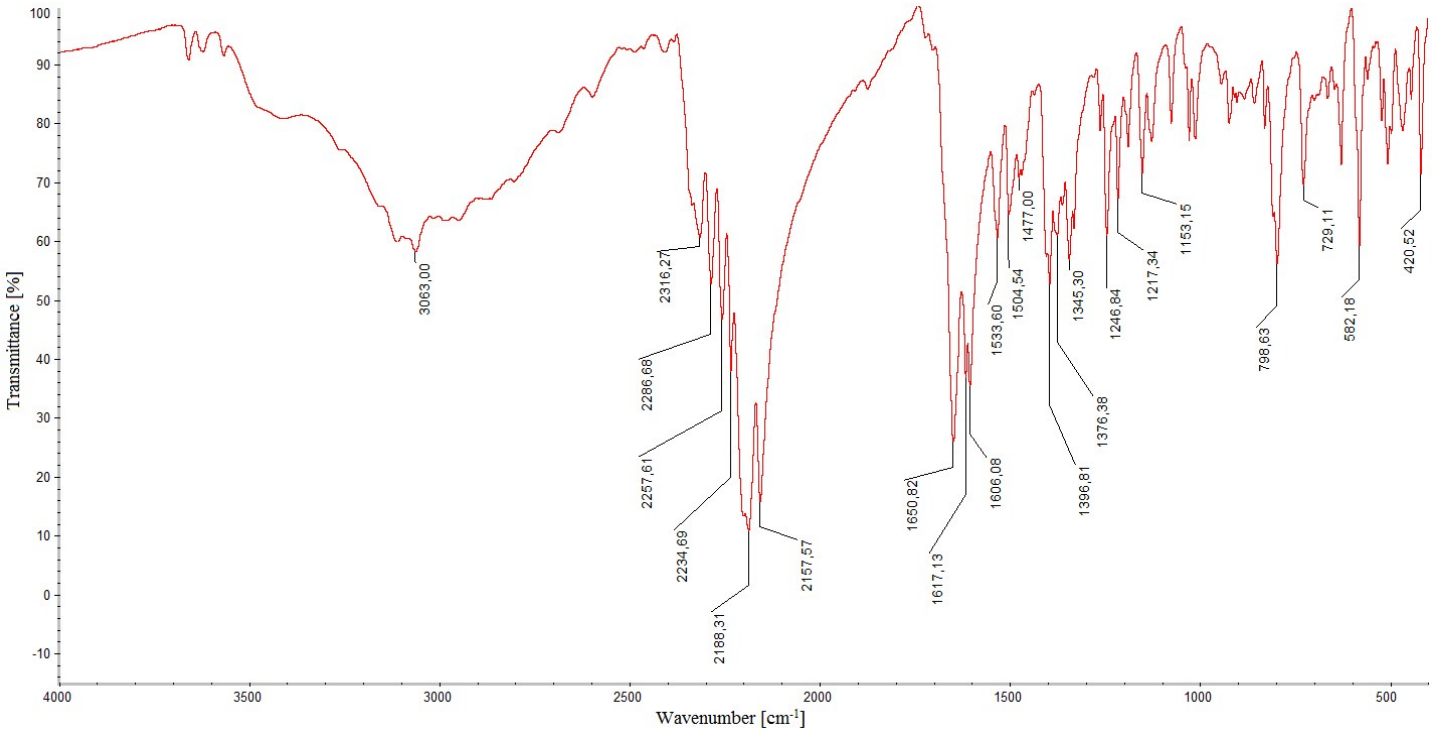

Figure S4. IR spectrum of **2**.

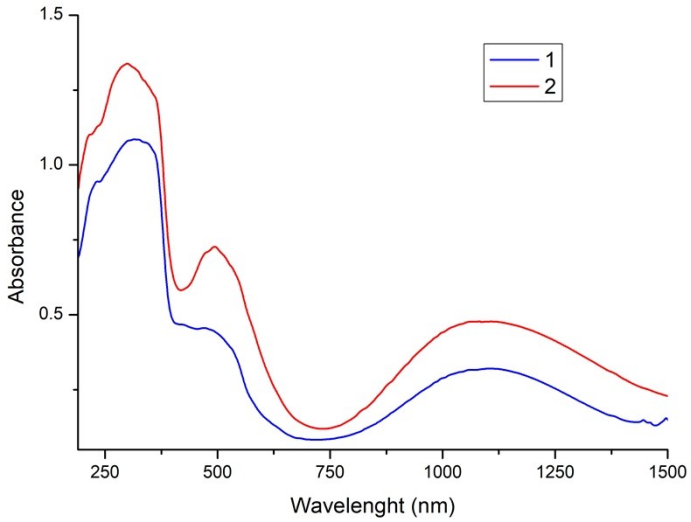

Figure S5. UV-Vis spectra of powder samples of **1** and **2**.

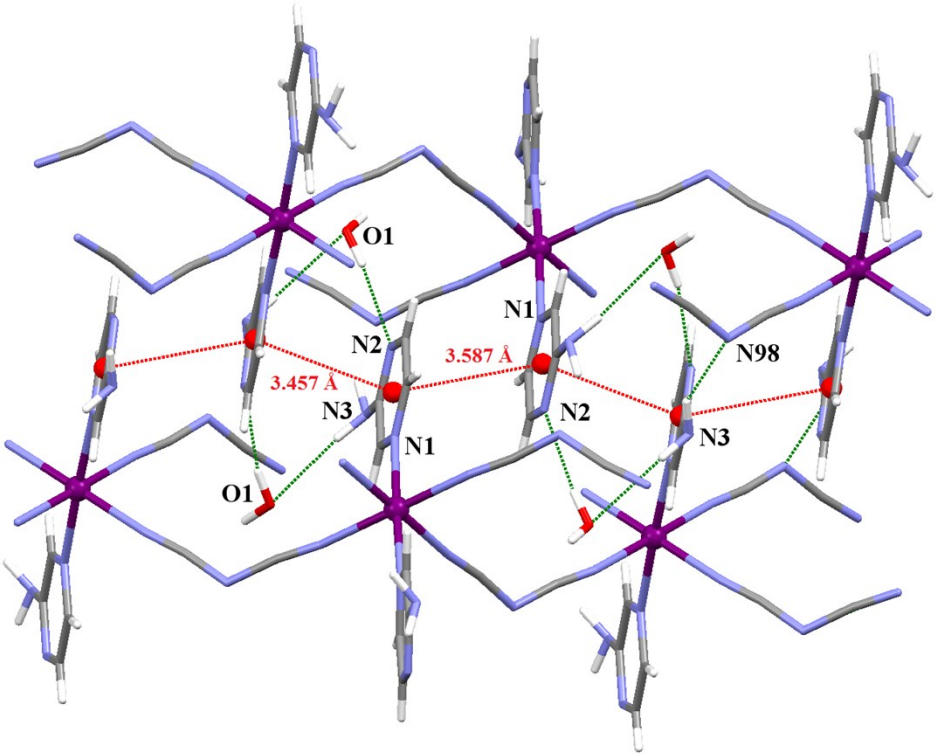

Figure S6. Crystal packing of **1** showing the hydrogen bonds (green dashed lines) and π⋯π stacking interactions (red dashed lines).

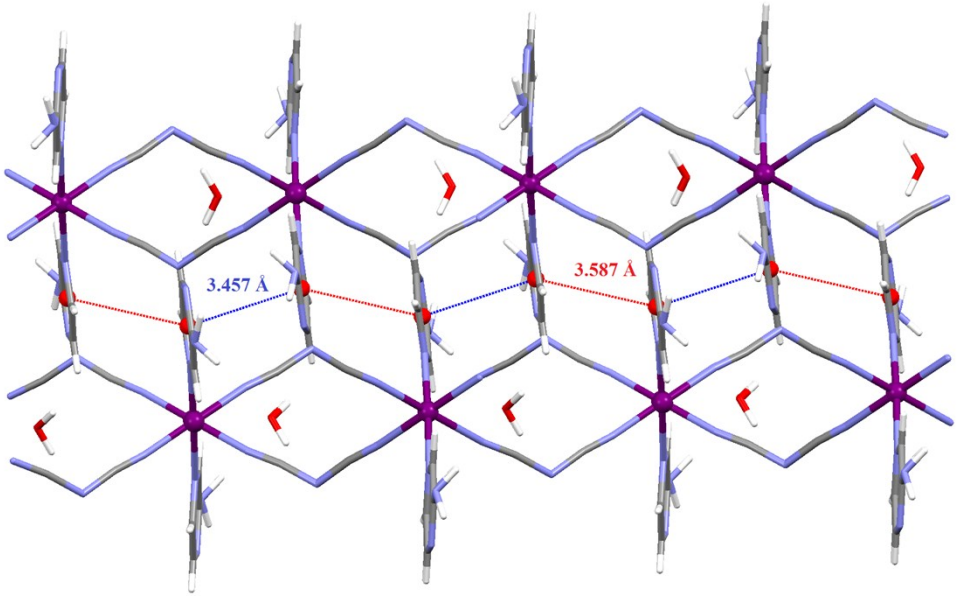

Figure S7. View of a fragment of the supramolecular 3D structure of **1**.

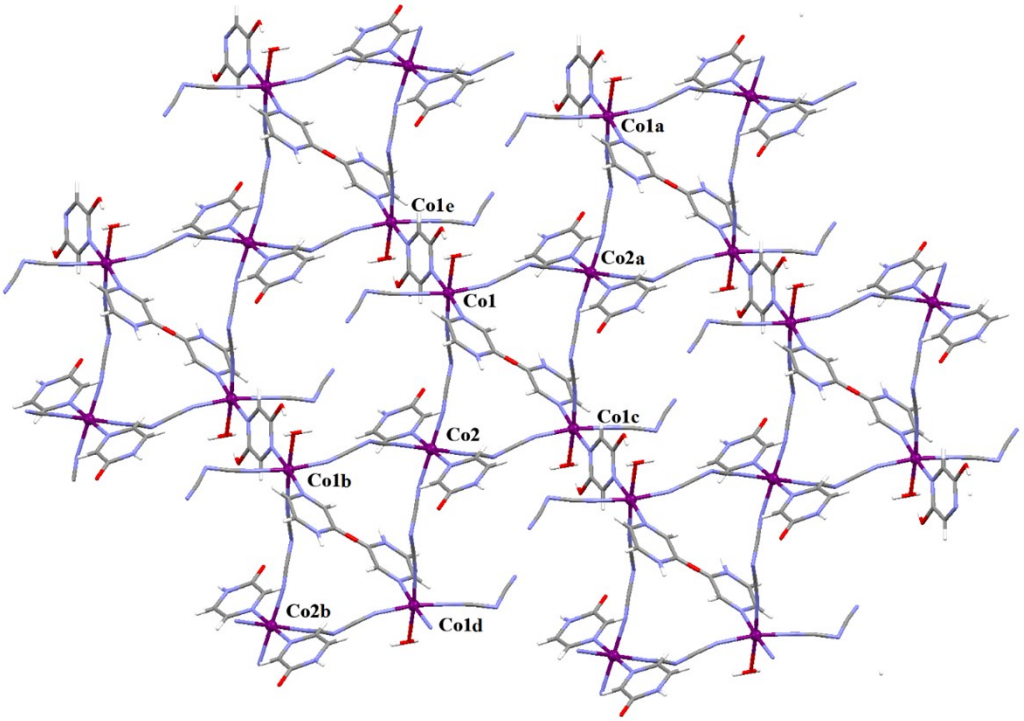

Figure S8. Two-dimensional coordination network of **2** formed by $\mu_{1,5}$-dca and HO*pyz* bridges [symmetry codes: (a) = *x*, –1+*y*, *z*, : (b) = *x*, 1+*y*, *z*; (c) = –*x*, –*y*, –*z*; (d) = –*x*, 1–*y*, –*z* and (e) = 2–*x*, –*y*, –*z*];

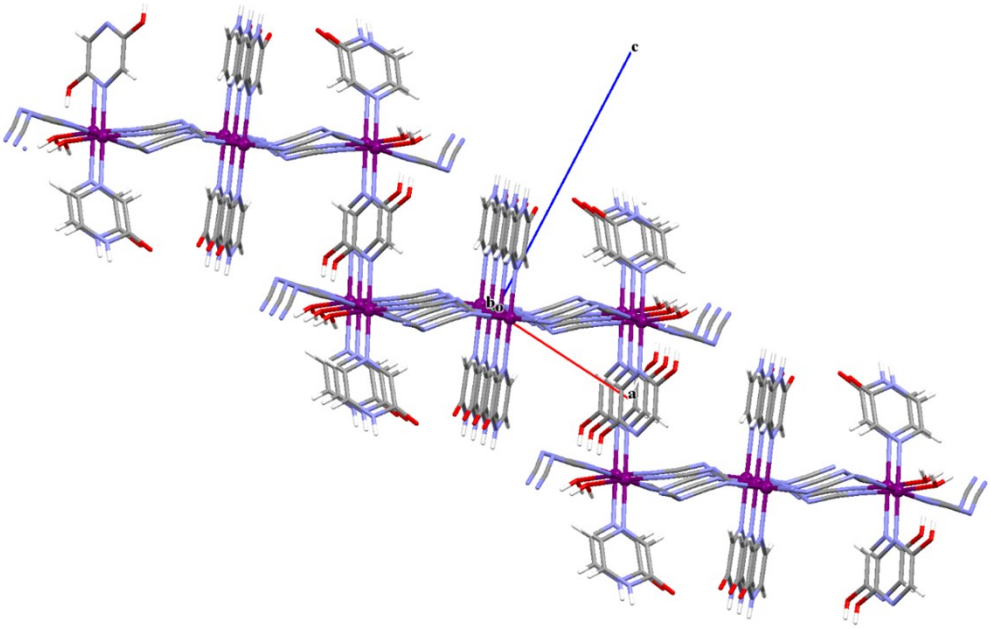

Figure S9. Side view illustrating the 2D stair-like network of **2.**

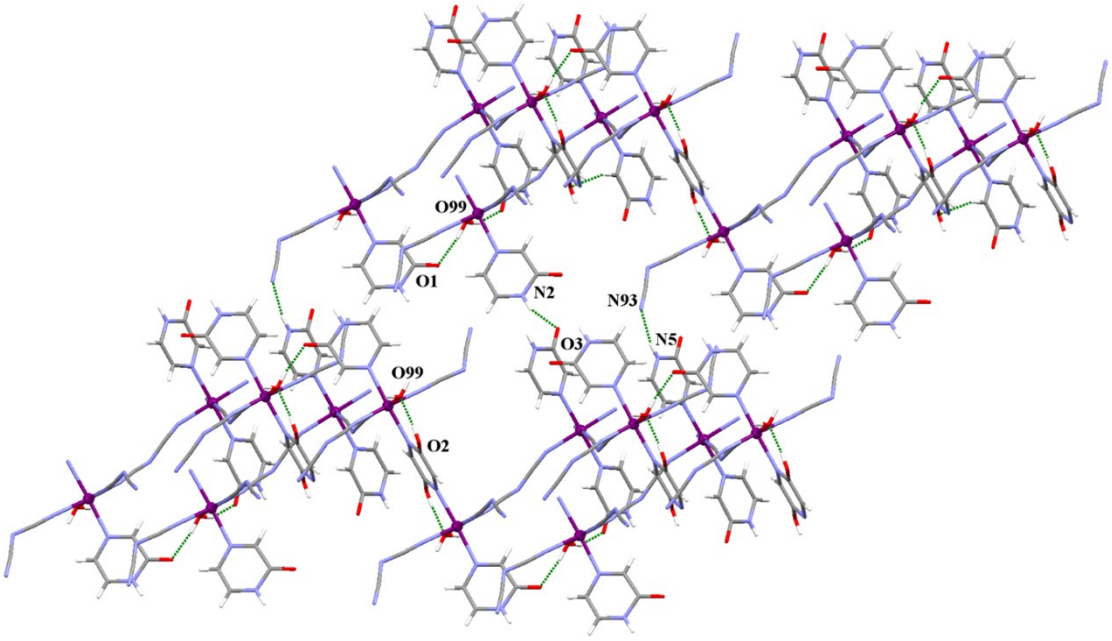

Figure S10. Crystal packing of **2** showing the hydrogen bonds.

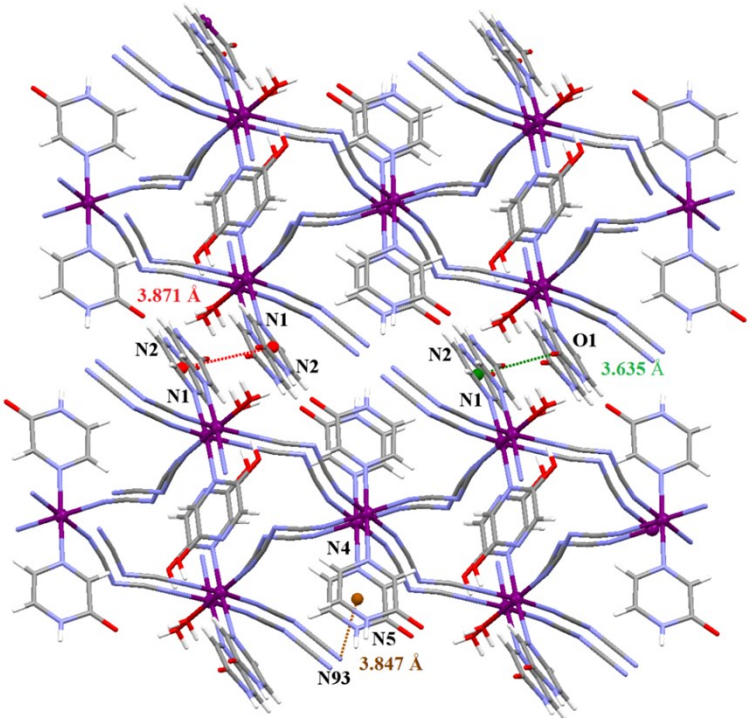

Figure S11. View of a fragment of the crystal packing of **2** showing π–π stacking and C—X•••π (X = O, N) type interactions.

1 Co(1)	2 Co(1)	2 Co(2)
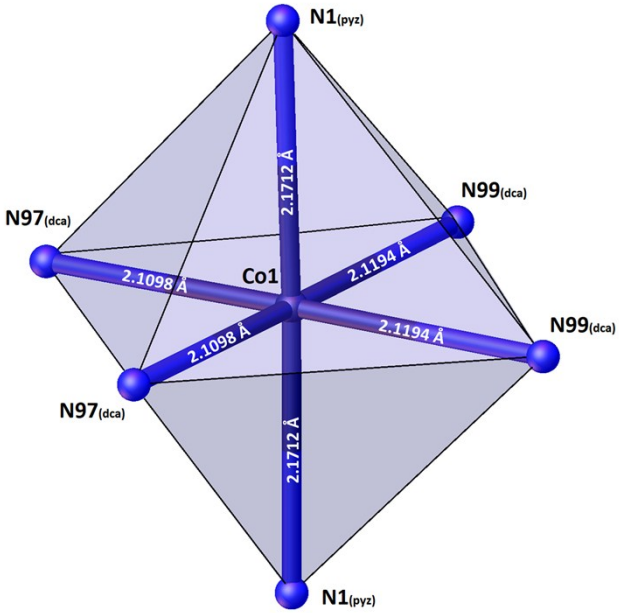	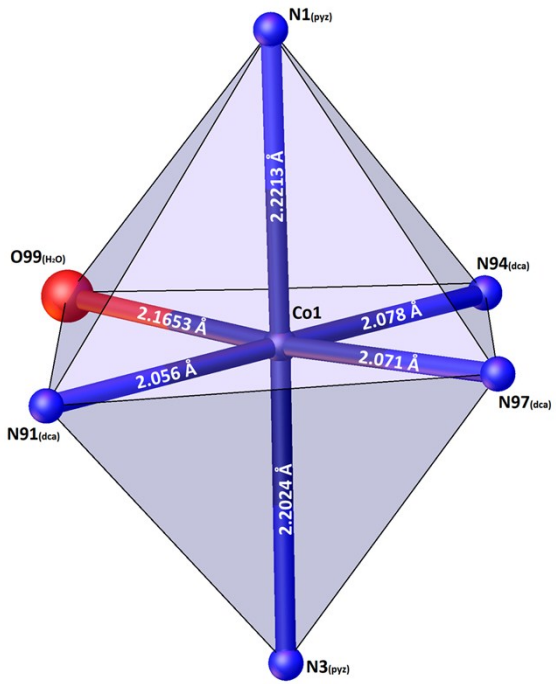	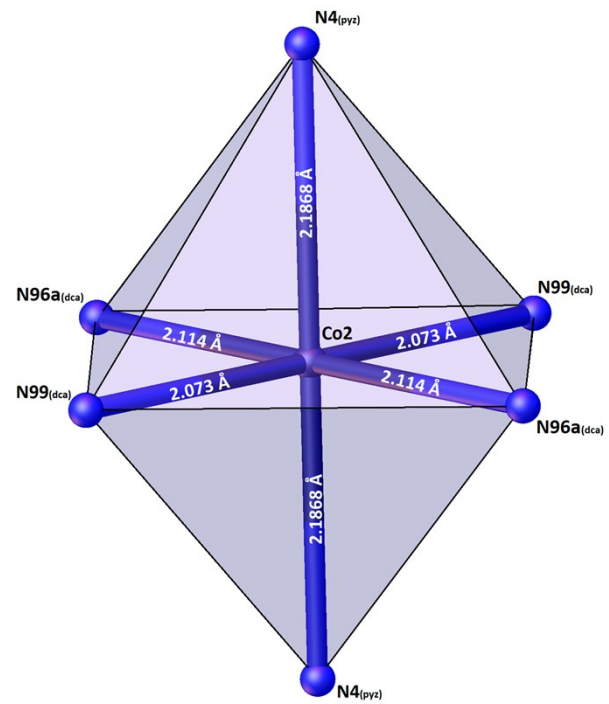
S(OC-6) = 0.052	S(OC-6) = 0.376	S(OC-6) = 0.066

Figure S12. The cobalt environment in **1**–**2** together with shape values (S_Q(P)) with respect to the octahedral geometry (OC-6), calculated with SHAPE program. The shape measure S_Q(P) is defined as $S_Q(P) = \min\left[(\sum_{i=1}^{n} |\vec{q}_i - \vec{p}_i|^2) / (\sum_{i=1}^{n} |\vec{q}_i - \vec{q}_0|^2) \right] \times 100$, where $\vec{q}_i$ are N vectors that contain the 3N Cartesian coordinates of the problem structure Q; $\vec{p}_i$ contain the coordinates of the ideal polyhedron P; $\vec{q}_0$ is the position vector of the geometric centre that is chosen to be the same for the two polyhedra. [M. Llunell, D. Casanova, J. Cirera, P. Alemany, S. Alvarez, *SHAPE version 2.0*., Universitat de Barcelona, **2010**; J. Cirera, P. Alemany and S. Alvarez, *Chem. Eur. J*., 2004, **10**, 190; D. Casanova, J. Cirera, M. Llunell, P. Alemany, D. Avnir and S. Alvarez, *J. Am. Chem. Soc*., 2004, **126**, 1755; J. Cirera, E. Ruiz and S. Alvarez, *Inorg. Chem*., 2008, **47**, 2871].

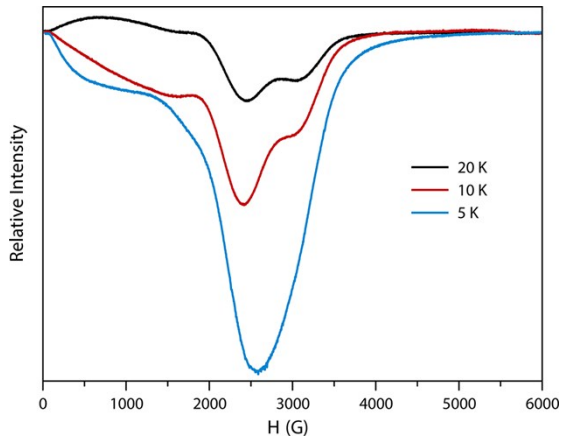

Figure S13. X-band EPR spectra on a powdered sample of **1** at the indicated temperatures.

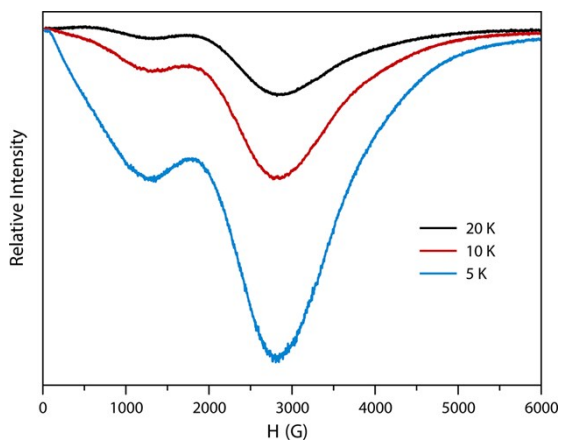

Figure S14. X-band EPR spectra on a powdered sample of **2** at the indicated temperatures.

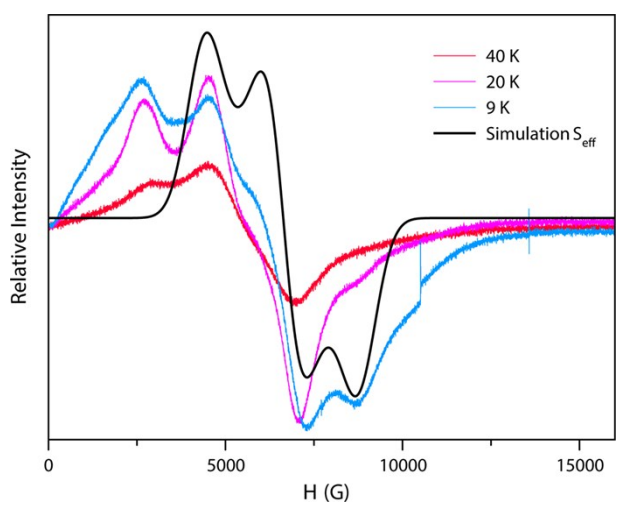

Figure S15. Q-band EPR spectra on a powdered sample of **2** at the indicated temperatures. The black trace corresponds to the best simulation for an effective spin S_{eff} = ½ (see text).

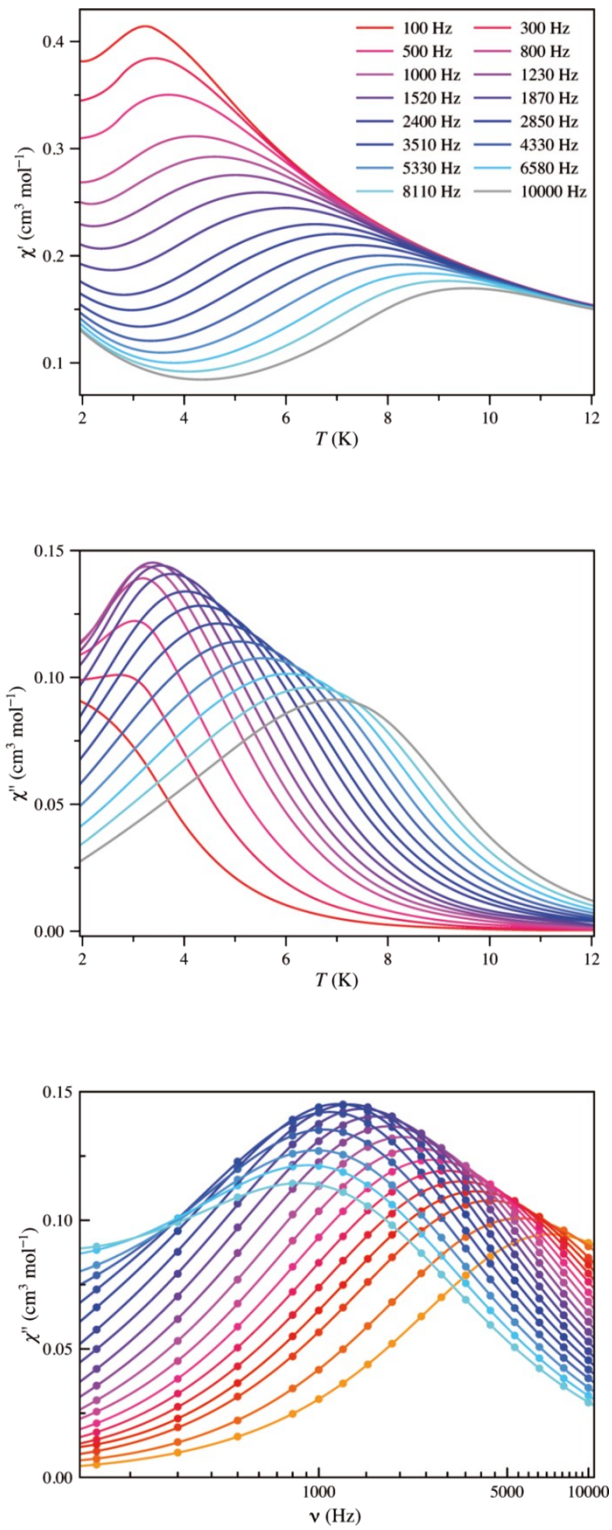

Figure S16. Thermal dependence of $\chi_{M'}$ (top) and $\chi_{M''}$ (middle) ac susceptibilities and frequency dependence of $\chi_{M''}$ (bottom) for **1** under an applied static field of H_{dc} = 1000 G with a ±5.0 G oscillating field at frequencies in the range 0.3-10 kHz.

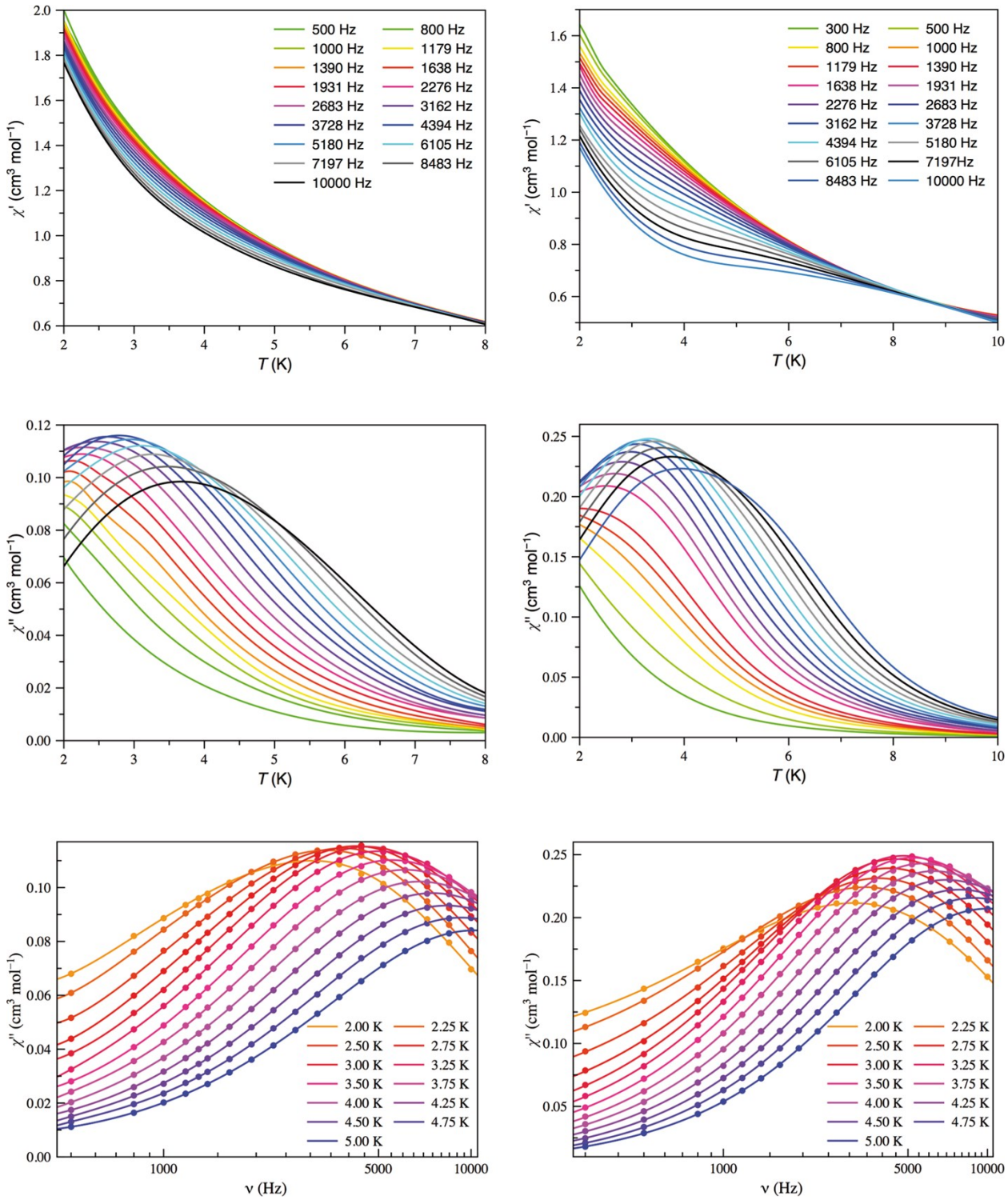

Figure S17. Thermal dependence of $\chi_{M'}$ (top) and $\chi_{M''}$ (middle) ac susceptibilities and frequency dependence of $\chi_{M''}$ (bottom) for **2** under an applied static fields of H_{dc} = 1000 (left) and 2000 G (right) with a ±5.0 G oscillating field at frequencies in the range 0.3-10 kHz.

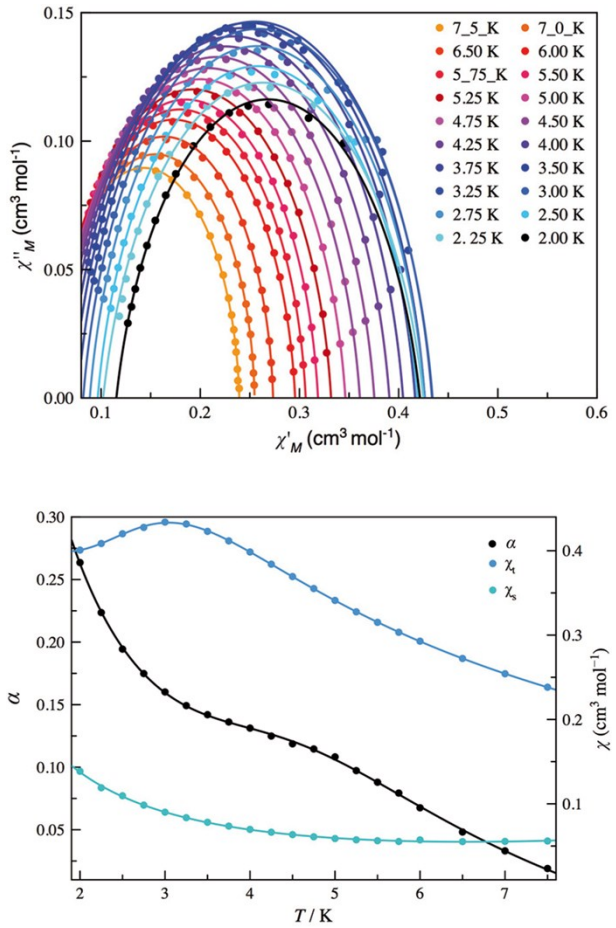

Figure S18. Cole-Cole plots (top) in the temperature range 2.0–7.5 K and the thermal dependence of the χ_t, χ_s and α parameters (bottom) for **1** under an applied static field of H_{dc} = 2500 G. The solid lines are the best-fit curves.

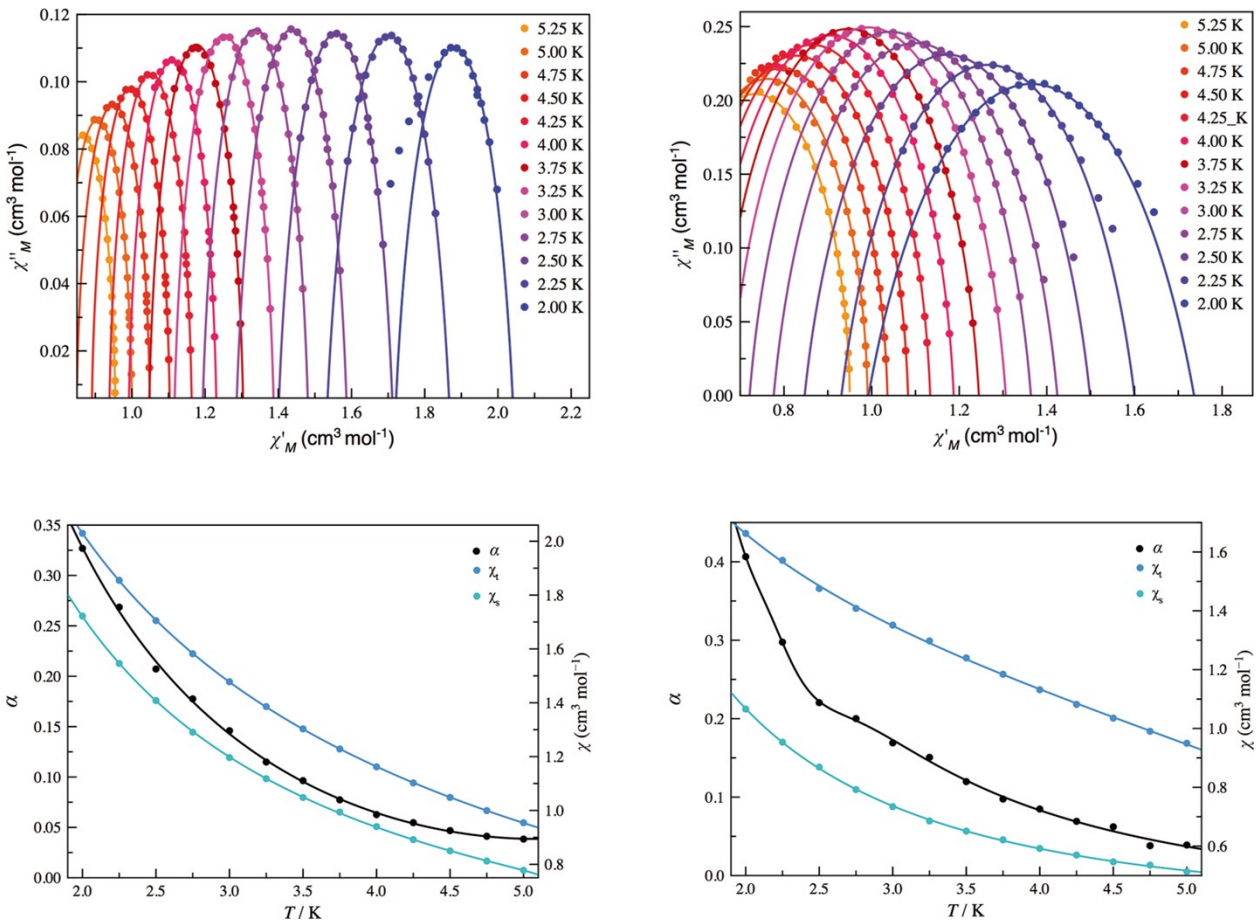

Figure S19. Cole-Cole plots (top) in the temperature range 2.0–5.25 K and the thermal dependence of the χ_t, χ_s and α parameters (bottom) for **2** under an applied static fields of H_{dc} = 1000 (left) and 2000 G (right). The solid lines are the best-fit curves.

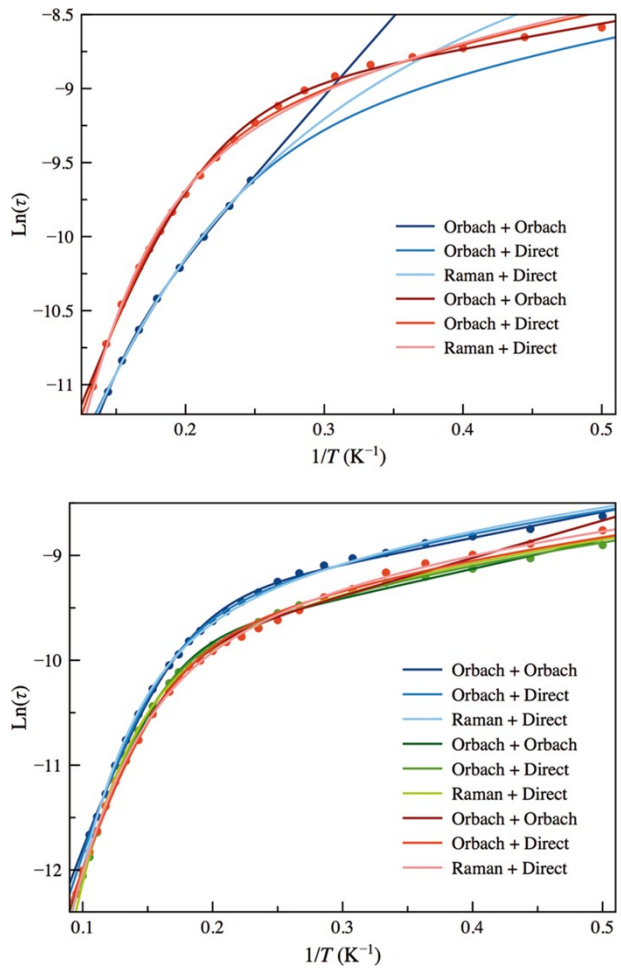

Figure S20. Arrhenius plots for **1** under an applied static field of H_{dc} = 2500 G obtained from temperature- (blue) and field- (red) dependences of $\chi_{M''}$ (top), and through the χ_M' *vs.* χ_M''/ϖ (blue), χ_M' *vs.* $\chi_M''\cdot\varpi$ (green) and χ_M''/ϖ *vs.* $\chi_M''\cdot\varpi$ (red) methods (bottom) which are described in the main text. The solid lines are the best-fit curves using Orbach-Orbach (dark), Orbach-direct (moderate) and Raman-direct (pale) approaches.

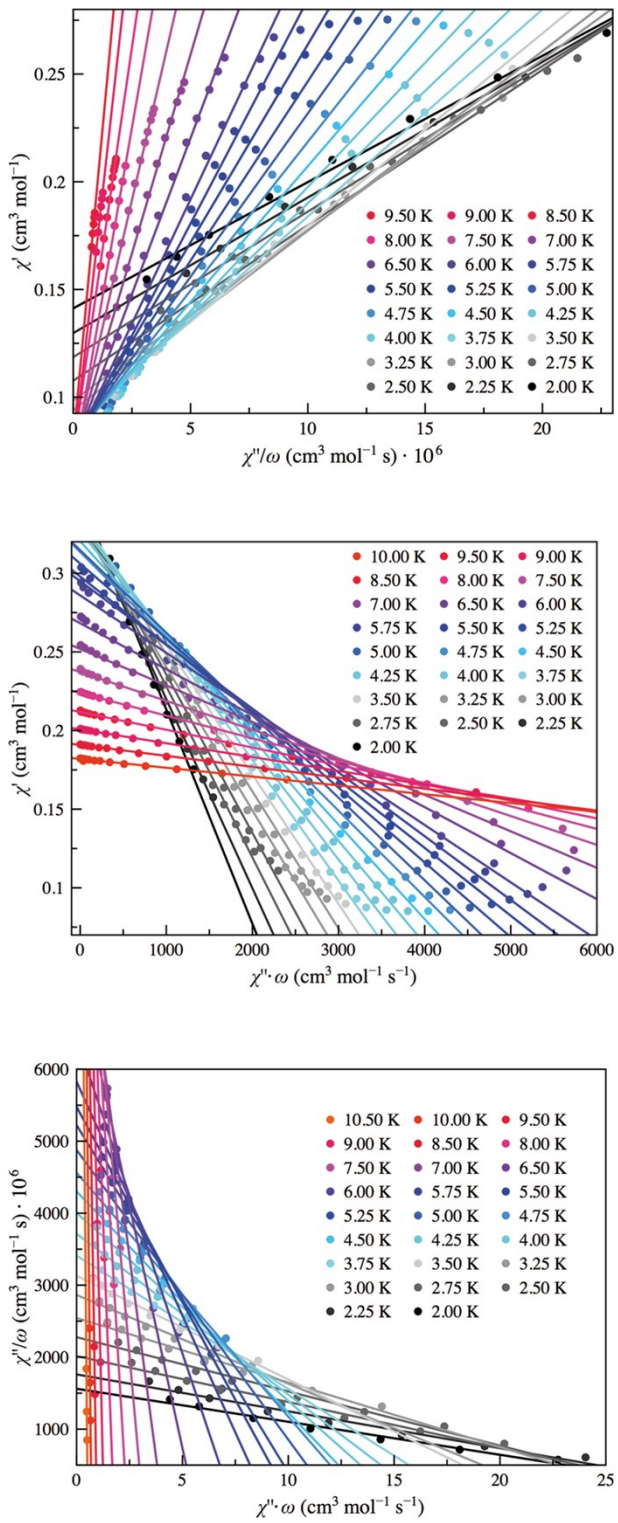

Figure S21. χ_M' against either χ_M''/ϖ (top) or $\chi_M''\cdot\varpi$ (middle) and χ_M''/ϖ *vs*. $\chi_M''\cdot\varpi$ plots for **1** under an applied static field of H_{dc} = 2500 G in the temperature range 2.0–10.5 K.

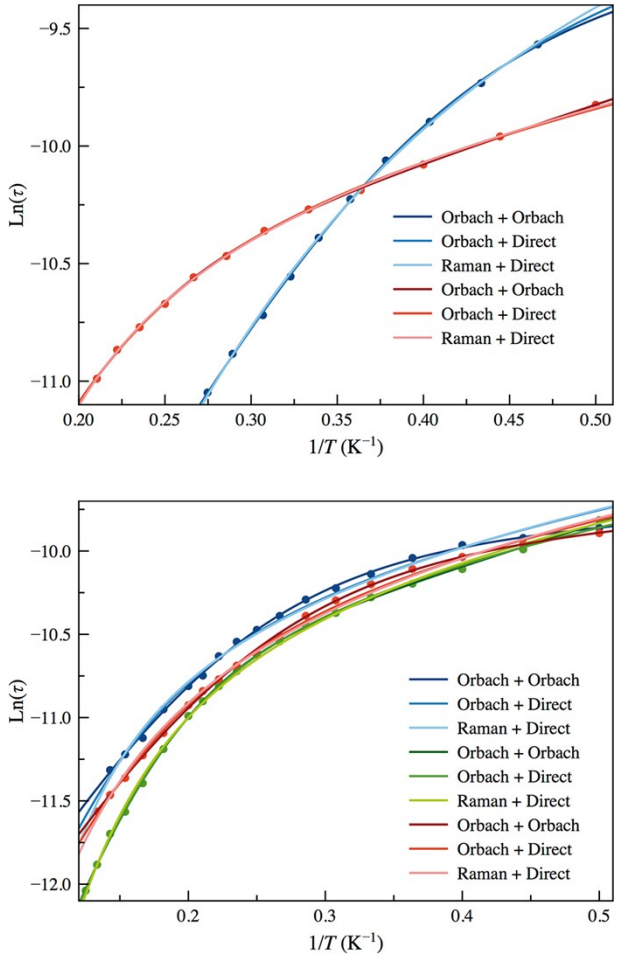

Figure S22. Arrhenius plots for **2** under an applied static field of H_{dc} = 1000 G obtained from temperature- (blue) and field- (red) dependences of $\chi_{M''}$ (top), and through the χ_M' *vs*. χ_M''/ϖ (blue), χ_M' *vs*. $\chi_M''\cdot\varpi$ (green) and χ_M''/ϖ *vs*. $\chi_M''\cdot\varpi$ (red) methods (bottom) which are described in the main text. The solid lines are the best-fit curves using Orbach-Orbach (dark), Orbach-direct (moderate) and Raman-direct (pale) approaches.

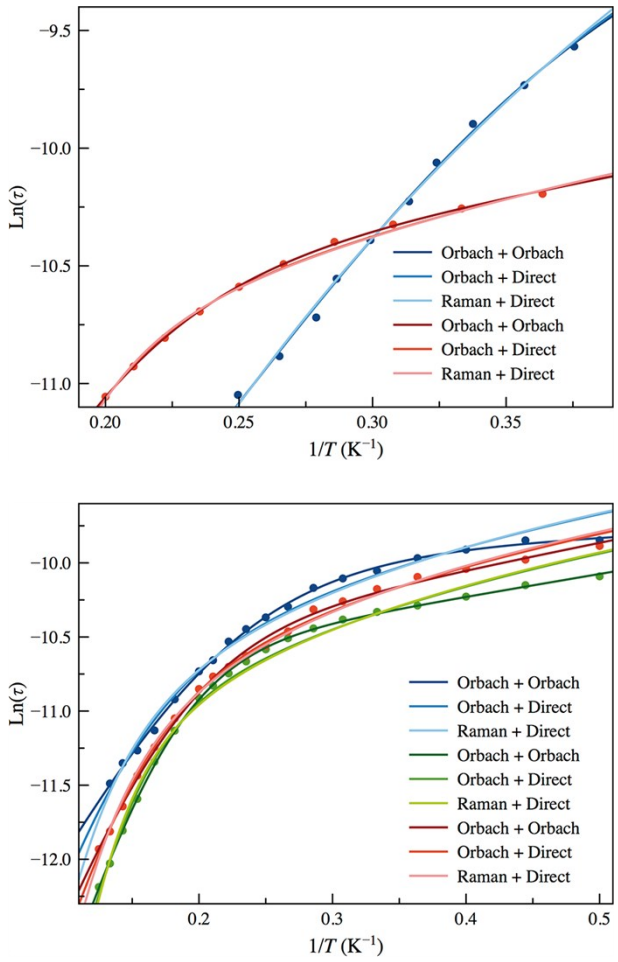

Figure S23. Arrhenius plots for **2** under an applied static field of H_{dc} = 2000 G obtained from temperature- (blue) and field- (red) dependences of $\chi_{M''}$ (top), and through the χ_M' *vs*. χ_M''/ϖ (blue), χ_M' *vs*. $\chi_M''\cdot\varpi$ (green) and χ_M''/ϖ *vs*. $\chi_M''\cdot\varpi$ (red) methods (bottom) which are described in the main text. The solid lines are the best-fit curves using Orbach-Orbach (dark), Orbach-direct (moderate) and Raman-direct (pale) approaches.

Table S1. Crystal data and structure refinement of **1** and **2.**

Compound	**1**	**2**
Empirical formula	$C_{12}H_{12}CoN_{12}O$	$C_{32}H_{23}Co_3N_{28}O_7$
Formula weight	399.27	1088.7
T [K]	295.0(2)	295.0(2)
Wavelength [Å]	0.71073	0.71073
Crystal system	Orthorhombic	Triclinic
Space group	*Pnna*	$P\bar{1}$
Unit cell dimensions [Å, º]		
a	13.5668(6)	6.9942(3)
b	12.9364(6)	12.0232(4)
c	9.2522(4)	12.8819(6)
α		93.330(3)
β		95.046(4)
γ		95.499(3)
V [Å^3]	1623.81(12)	1071.70(8)
Z	4	1
D_c [Mg m^{-3}]	1.633	1.687
Absorption coefficient [mm^{-1}]	1.090	1.231
F(000)	812.0	548.0
Crystal size [mm]	0.177×0.112×0.080	0.158×0.112×0.099
θ range for data collection [°]	3.39 to 25.05	3.41 to 25.05
Index ranges	$-15 \le h \le 16$ $-15 \le k \le 12$ $-8 \le l \le 11$	$-6 \le h \le 8$ $-14 \le k \le 12$ $-15 \le l \le 14$
Reflections collected	4437	7963
Independent reflections	1441(R_{int} = 0.0267)	3781 (R_{int} = 0.0228)
Completeness to 2θ [%]	99.7	99.8
Min. and max. transm.	0.860 and 1.000	0.677 and 1.000
Data/restraints/parameters	1441/0/123	3781/0/333
Goodness-of-fit on F^2	1.030	1.035
Final R indices [$I > 2\sigma(I)$]		
$R1$	0.0293	0.0304
$wR2$	0.0742	0.0676
R indices (all data)		
$R1$	0.0386	0.0381
$wR2$	0.0789	0.0703
Largest diff. peak/hole [e Å^{-3}]	0.29 and -0.22	0.28 and -0.25

Table S2. Selected bond lengths (Å) and angles (deg) for **1**.

Bond lengths		Bond angles	
Co(1)–N(1)	2.1712(17)	N(1)–Co(1)–N(1e)	178.36(9)
Co(1)–N(97)	2.1098(18)	N(1)–Co(1)–N(97)	88.18(6)
Co(1)–N(99)	2.1194(18)	N(1)–Co(1)–N(99)	90.84(6)
		N(1)–Co(1)–N(97e)	90.68(6)
		N(1)–Co(1)–N(97e)	90.33(6)
		N(97)–Co(1)–N(97e)	92.18(10)
		N(97)–Co(1)–N(99)	89.63(7)
		N(97)–Co(1)–N(99e)	177.67(7)
		N(99)–Co(1)–N(99e)	88.60(10)
		Co(1)–N(97)–C(98)	173.67(17)
		Co(1)–N(99)–C(99)	169.84(18)
		N(97)–C(98)–N(98)	172.6(2)
		C(98)–N(98)–C(99b)	122.31(19)

Symmetry transformations used to generate equivalent atoms: (b) = 1/2+*x*, *y*, 1–*z*; (e) = *x,* 1/2–*y*, 3/2–*z*.

Table S3. Selected bond lengths (Å) and angles (deg) for **2**.

Bond lengths		Bond angles	
Co(1)–N(1)	2.2213(18)	N(1)–Co(1)–N(3)	175.82(7)
Co(1)–N(3)	2.2024(18)	N(1)–Co(1)–N(91)	90.95(7)
Co(1)–N(91)	2.056(2)	N(1)–Co(1)–N(94)	92.42(7)
Co(1)–N(94)	2.078(2)	N(1)–Co(1)–N(97)	86.15(7)
Co(1)–N(97)	2.071(2)	N(1)–Co(1)–O(99)	91.20(7)
Co(1)–O(99)	2.1653(16)	N(3)–Co(1)–N(91)	85.96(7)
Co(2)–N(4)	2.1868(19)	N(3)–Co(1)–N(94)	91.07(7)
Co(2)–N(96a)	2.114(2)	N(3)–Co(1)–N(97)	91.42(7)
Co(2)–N(99)	2.073(2)	N(3)–Co(1)–O(99)	91.45(7)
		N(91)–Co(1)–N(94)	170.58(9)
		N(91)–Co(1)–N(97)	97.02(9)
		N(91)–Co(1)–O(99)	86.97(7)
		N(94)–Co(1)–N(97)	91.98(8)
		N(94)–Co(1)–O(99)	84.17(7)
		N(97)–Co(1)–O(99)	175.24(7)
		N(4)–Co(2)–N(4d)	180.0
		N(4)–Co(2)–N(96b)	88.42(8)
		N(4)–Co(2)–N(96c)	91.58(8)
		N(4d)–Co(2)–N(96b)	91.57(8)
		N(4d)–Co(2)–N(96c)	88.43(8)
		N(4)–Co(2)–N(99)	91.12(8)
		N(4)–Co(2)–N(99d)	88.88(8)
		N(96c)–Co(2)–N(96b)	180.00(12)
		N(96c)–Co(2)–N(99)	90.37(9)
		N(96c)–Co(2)–N(99d)	89.63(9)
		N(99d)–Co(2)–N(99)	180.0
		Co(1)–N(91)–C(94)	174.0(2)
		Co(1)–N(94)–C(96)	167.2(2)
		Co(1)–N(97)–C(98)	170.2(2)
		Co(2)–N(99)–C(99)	166.4(2)
		Co(2b)–N(96)–C(97)	159.4(2)
		N(91)–C(94)–N(92)	174.2(3)
		N(93)–C(95)–N(92)	173.6(4)
		N(94)–C(96)–N(95)	171.9(3)
		N(96)–C(97)–N(95)	172.4(3)
		N(97)–C(98)–N(98)	171.3(3)
		N(99)–C(99)–N(98)	171.5(3)
		C(94)–N(92)–C(95)	120.2(2)
		C(96)–N(95)–C(97)	123.8(2)
		C(98)–N(99)–C(99)	126.8(2)

Symmetry transformations used to generate equivalent atoms: (a) = x, $-1+y$, z; (b) = x, $1+y$, z; (c) = $-x$, $-y$, $-z$; (d) = $-x$, $1-y$, $-z$.

Table S4. Hydrogen bonds and C–H···N type interactions in **1** and **2**[a]

D	A	D—H [Å]	H···A [Å]	D···A [Å]	D—H···A [°]
			1		
O(1)	N(2)[f]	0.85	2.37	3.190(2)	162.0
O(1)	N(2)	0.85	2.47	3.190(2)	143.0
N(3)	O(1)[g]	0.86	2.32	3.137(3)	158.0
N(3)	N(98)[i]	0.86	2.37	3.130(3)	147.0
C(4)	N(98)[j]	0.93	2.58	3.470(3)	159.0
			2		
O(2)	O(99)	0.82	1.68	2.500(4)	175.0
N(2)	O(3)[k]	0.85	2.02	2.813(3)	157.0
N(5)	N(93)[l]	0.80	2.21	2.2975(4)	161.0
O(99)	O(3)[m]	0.87	2.26	3.066(2)	154.0
O(99)	O(1)[n]	0.87	2.44	2.963(2)	119.0
O(99)	O(1)[o]	0.87	1.80	2.667(2)	170.0
C(1)	N(94)	0.93	2.61	3.188(3)	121.0
C(6)	N(97)	0.93	2.49	3.093(3)	122.0

[a] Symmetry transformations used to generate equivalent atoms: (f) = *x*, 3/2–*y*, 1/2–*z*, (g) = 1/2–*x*, 1-*y*, *z*; (h) = 1-*x*,1/2+ *y*, –1/2+*z*; (i) = 1–*x*, 1/2+*y*, 1/2+*z*; (j) = 2–*x*,–*y*,–*z*; (k) = 1–*x*, 1–*y*, 1–*z*; (l) = 1+*x*, –1+*y*, *z*; (m) = 1–*x*, –*y*, 1–*z*; (n) = 1+*x*, *y*, *z*; (o) = 1/2–*x*, –1/2+*y*, 3/2–*z*.

Table S5. Short π···π interactions for **1** and **2**[a]

Cg(I)···Cg(J)	Cg(I)···Cg(J) [Å]	α [°][b]	β[°][c]	γ [°][d]	Cg(I)–Perp [Å][e]	Cg(J)–Perp [Å][f]
			1			
Cg(1)···Cg(1q)[g]	3.4575(12)	8	12.11	12.11	-3.3805(8)	-3.3805(8)
Cg(1)···Cg(1p)	3.5870(12)	0	19.81	19.81	3.3748(8)	3.3748(8)
			2			
Cg(1)···Cg(1r)	3.8706(12)	0	30.49	30.49	-3.3352(9)	-3.3352(9)

[a] Symmetry code: (q) = 1/2–*x*, 1–*y*, *z*; (p) = 1–*x*, 1–*y*, 1–*z*; (r) = 1–*x*, –*y*, 1–*z*; (s) = 3/2–*x*, –1/2+*y*, 3/2–*z*. [b] α = dihedral angle between Cg(I) and Cg(J). [c]β = angle Cg(I)→Cg(J) vector and normal to ring I. [d] γ = angle between the Cg(I)→Cg(J) vector and the normal to plane J. [e] Cg(I)–Perp = Perpendicular distance of Cg(I) on ring J. [f] Cg(J)–Perp = perpendicular distance of Cg(J) on ring I. [g] Cg1 is the centroid of the N(1)/C(1)/C(2)/N(2)/C(3)/C(4) set of atoms.

Table S6. C—X···Cg(J)(π-ring) (X = O, N) interactions for **2**[a]

C–X(I)···Cg(J)	X(I)···Cg(J) [Å]	X-Perp [Å]	γ [°][b]
C(2)-O(1)···Cg(1r)[c]	3.6346(19)	-3.224	27.49
C(95)-N(93)···Cg(2t)[d]	3.847(3)	3.755	12.56

[a] Symmetry codes: (r) = 1–*x*, –*y*, 1–*z*; (t) = 1+*x*, *y*, *z*. [b] γ = angle X(I)→Cg(J) vector and normal to plane J. [c] Cg1 is the centroid of the N(1)/C(1)/C(2)/N(2)/C(3)/C(4) set of atoms. [d]Cg2 is the centroid of the N(4)/C(7)/C(8)/N(5)/C(9)/C(10) set of atoms.

Table S7. Energy of all calculated excited states and their contributions to the *D* and *E* values for the real geometries of Co1 in **1** and Co2 in **2** obtained from CASSCF/NEVPT2 calculations.

Co1 in **1**					Co2 in **2**				
State	Energy[a]	*S*	*D*[a]	*E*[a]	State	Energy[a]	*S*	*D*[a]	*E*[a]
D_{SS}		4	1.874	0.007	D_{SS}		4	1.762	0.046
D_Q		4	80.905	16.961	D_Q		4	81.737	15.839
D_D		2	14.527	–0.129	D_D		2	12.425	0.582
Q_1	564.7	4	43.604	43.620	Q_1	581.4	4	44.434	43.241
Q_2	1089.3	4	26.264	–26.264	Q_2	973.9	4	29.632	–27.792
Q_3	9461.7	4	5.838	–5.838	Q_3	9204.4	4	0.879	–0.549
Q_4	9636.2	4	4.172	4.476	Q_4	9470.1	4	3.645	1.632
Q_5	9822.5	4	0.898	0.979	Q_5	10213.4	4	3.053	–0.682
Q_6	19845.4	4	0.000	0.000	Q_6	20065.4	4	–0.001	0.000
Q_7	22730.4	4	0.070	–0.070	Q_7	22104.0	4	0.048	–0.027
Q_8	22776.0	4	0.058	0.059	Q_8	23095.5	4	0.041	0.010
Q_9	24441.7	4	0.001	–0.001	Q_9	25006.9	4	0.006	0.006
D_1	10559.8	2	12.521	–0.113	D_1	9666.7	2	10.712	0.778
D_2	11404.9	2	–0.046	0.046	D_2	11856.5	2	0.279	–0.213
D_3	19187.2	2	–0.001	0.001	D_3	18537.4	2	–0.016	–0.014
D_4	19760.1	2	–1.136	–1.136	D_4	19054.1	2	–0.090	0.073
D_5	19809.4	2	–0.667	0.667	D_5	19436.2	2	–0.867	–0.584
D_6	19873.5	2	–0.087	–0.088	D_6	20021.1	2	–0.848	0.014
D_7	19897.1	2	–0.010	–0.010	D_7	20277.2	2	–0.510	0.481
D_8	20240.6	2	–0.513	0.513	D_8	20480.4	2	–0.018	0.018
D_9	22728.8	2	3.228	0.000	D_9	22939.5	2	2.780	0.004
D_{10}	23546.5	2	–0.002	0.002	D_{10}	23086.3	2	–0.133	–0.104

D_{11}	23573.1	2	–0.105	–0.106	D_{11}	23566.0	2	–0.057	–0.046
D_{12}	26811.2	2	–0.116	0.116	D_{12}	26870.6	2	–0.122	0.114
D_{13}	29647.4	2	–0.191	0.191	D_{13}	29565.4	2	0.053	0.018
D_{14}	29898.0	2	–0.060	–0.072	D_{14}	29829.2	2	0.024	0.001
D_{15}	30061.2	2	–0.026	–0.041	D_{15}	30213.0	2	–0.032	0.057
D_{16}	31480.3	2	–0.405	0.405	D_{16}	31536.9	2	–0.047	–0.048
D_{17}	31565.3	2	–0.492	–0.496	D_{17}	31617.3	2	–0.562	0.158
D_{18}	31903.3	2	–0.003	0.003	D_{18}	31897.0	2	–0.547	–0.220
D_{19}	32642.1	2	2.644	–0.017	D_{19}	32760.7	2	2.377	0.124
D_{20}	33504.8	2	–0.006	0.006	D_{20}	33371.4	2	0.049	–0.029

[a]Values in cm^{-1}.

Table S8. Energy of all calculated excited states and their contributions to the *D* and *E* values for the real geometries of Co1 and Co1e in **2** obtained from CASSCF/NEVPT2 calculations.

Co1					Co1e				
State	Energy[a]	*S*	*D*[a]	*E*[a]	State	Energy[a]	*S*	*D*[a]	*E*[a]
D_{SS}		4	1.859	0.046	D_{SS}		4	1.857	0.052
D_Q		4	92.234	19.658	D_Q		4	95.549	29.759
D_D		2	14.383	–0.114	D_D		2	14.569	–0.166
Q_1	521.0	4	49.809	49.270	Q_1	389.7	4	56.517	56.487
Q_2	820.0	4	31.029	–30.073	Q_2	925.7	4	27.254	–27.199
Q_3	8533.2	4	4.800	4.895	Q_3	8465.7	4	5.852	6.028
Q_4	8746.7	4	1.198	0.801	Q_4	8791.2	4	0.256	0.002
Q_5	9644.5	4	5.304	–5.225	Q_5	9578.7	4	5.572	–5.548
Q_6	18748.0	4	–0.009	–0.000	Q_6	18766.4	4	–0.012	–0.000
Q_7	21237.8	4	0.056	–0.054	Q_7	20999.6	4	0.060	–0.060
Q_8	23098.7	4	0.045	0.044	Q_8	23452.4	4	0.049	0.049
Q_9	24140.1	4	0.002	0.000	Q_9	24008.8	4	0.001	0.000
D_1	10220.6	2	10.858	0.023	D_1	10109.9	2	10.393	–0.009
D_2	12439.4	2	1.617	–0.042	D_2	12452.6	2	2.221	–0.053
D_3	18373.6	2	–0.002	0.002	D_3	18348.3	2	–0.001	0.001
D_4	19008.1	2	–0.005	0.003	D_4	18963.9	2	–0.003	0.000
D_5	19479.3	2	–1.134	–1.105	D_5	19349.9	2	–1.159	–1.152
D_6	20157.4	2	–1.180	1.120	D_6	20157.5	2	–0.851	0.840
D_7	20216.7	2	–0.087	0.044	D_7	20220.2	2	–0.367	0.360
D_8	20245.6	2	–0.025	0.017	D_8	20268.7	2	–0.078	0.073
D_9	22581.6	2	2.967	–0.001	D_9	22532.2	2	3.026	–0.000
D_{10}	23009.8	2	–0.011	–0.011	D_{10}	22855.4	2	–0.004	–0.005

D_{11}	23541.5	2	–0.211	–0.210	D_{11}	23620.0	2	–0.213	–0.216
D_{12}	26231.1	2	–0.073	0.073	D_{12}	26232.0	2	–0.052	0.052
D_{13}	29192.8	2	–0.000	0.007	D_{13}	29255.9	2	–0.011	0.021
D_{14}	29369.1	2	–0.010	0.012	D_{14}	29373.4	2	0.002	0.001
D_{15}	29896.4	2	–0.145	0.169	D_{15}	29833.8	2	–0.205	0.213
D_{16}	30961.8	2	–0.272	–0.267	D_{16}	30842.7	2	–0.557	–0.545
D_{17}	30974.0	2	–0.365	–0.306	D_{17}	31066.6	2	–0.172	0.043
D_{18}	31155.7	2	–0.365	0.363	D_{18}	31073.1	2	–0.212	0.218
D_{19}	32129.9	2	2.544	–0.001	D_{19}	32007.6	2	2.383	–0.003
D_{20}	32897.5	2	0.282	–0.004	D_{20}	32964.6	2	0.429	–0.005

[a]Values in cm^{-1}.

Table S9. Energies of the low-lying Kramers doublets corresponding to the ground and first excited states, which should be related to those generated from the 1st order spin-orbit coupling, of the real geometries of Co1 in **1** and Co1, Co1e and Co2 in **2** obtained from CASSCF/NEVPT2 calculations.

Kramers doublet	Energy[a]			
	Co1 in **1**	Co2 in **2**	Co1 in **2**	Co1e in **2**
Ground	0.0	0.0	0.0	0.0
1st	196.2	196.9	220.1	239.4
2nd	720.5	737.9	687.4	639.9
3rd	1029.9	1055.0	1040.1	975.3
4th	1461.2	1368.4	1275.6	1381.0
5th	1556.1	1467.6	1360.6	1436.6

[a]Values in cm^{-1}.

Table S10. Selected ac magnetic data for **1** under H_{dc} = 1000 G

Method	Model[a]	τ_{01}[b] × 10^7 (s)	E_{a1}[b] (cm^{-1})	τ_{02}[b] × 10^5 (s)	E_{a2}[b] (cm^{-1})	A[c] (s^{-1} K^{-1})	C[d] (s^{-1} K^{-n})	n[d]
χ_M' *vs.* T	O-O	14.7 ± 1.44	9.2 ± 0.4	13 ± 6	0.4 ± 0.6			
	O-D	13.1 ± 0.3	10.26 ± 0.21			3090 ± 70		
	R-D					1600 ± 400	330 ± 120	3.00 ± 0.18
χ_M' *vs.* ν	O-O	9.66 ± 0.05	14.2 ± 0.3	3.20 ± 0.15	2.71 ± 0.07			
	O-D	17.8 ± 1.8	11.5 ± 0.4			2350 ± 60		
	R-D					1580 ± 30	170 ± 8	3.065 ± 0.023
χ_M' *vs.* χ_M''/ϖ	O-O	7.7 ± 1.0	17.8 ± 0.8	2.66 ± 0.25	2.81 ± 0.16			
	O-D	13.7 ± 1.5	14.6 ± 0.6			2900 ± 90		
	R-D					2110 ± 100	140 ± 22	2.89 ± 0.07
χ_M' *vs.* χ_M''·ϖ	O-O	2.6 ± 0.4	21.81 ± 0.10	2.01 ± 0.18	2.66 ± 0.16			
	O-D	3.8 ± 0.6	19.7 ± 0.9			4370 ± 110		
	R-D					3850 ± 70	25 ± 4	3.84 ± 0.07
χ_M''/ϖ *vs.* χ_M''·ϖ	O-O	4.7 ± 0.7	19.0 ± 1.0	1.93 ± 0.20	3.04 ± 0.18			
	O-D	9.1 ± 1.2	15.2 ± 0.7			3540 ± 120		
	R-D					2660 ± 90	131 ± 17	3.05 ± 0.06

[a] O-O, O-D, and R-D stand for Orbach-Orbach, Orbach-Direct, and Raman-Direct combinations, respectively. [b] The values of the preexponential factor (τ_0) and activation energy (E_a) are calculated through the Arrhenius law [$\tau^{-1} = \tau_0^{-1} \exp(-E_a/k_BT)$]. [c] The preexponential coefficient for the Direct mechanism [$\tau^{-1} = AT$]. [d] The preexponential and exponential coefficients for the Raman mechanism [$\tau^{-1} = CT^n$].

Table S11. Selected ac magnetic data for **1** under H_{dc} = 2500 G

Method	Model[a]	τ_{01}[b] × 10^7 (s)	E_{a1}[b] (cm^{-1})	τ_{02}[b] × 10^5 (s)	E_{a2}[b] (cm^{-1})	A[c] (s^{-1} K^{-1})	C[d] (s^{-1} K^{-n})	n[d]
χ_M' *vs.* T	O-O	0.29 ± 0.13	37 ± 3	0.47 ± 0.04	7.44 ± 0.22			
	O-D	7.7 ± 1.7	16.6 ± 1.2			2920 ± 21		
	R-D					1500 ± 400	100 ± 50	3.22 ± 0.22
χ_M' *vs.* ν	O-O	5.8 ± 0.8	18.8 ± 0.6	8.3 ± 0.6	1.17 ± 0.13			
	O-D	2.5 ± 0.6	24.0 ± 1.0			2410 ± 40		
	R-D					2350 ± 50	0.5 ± 0.3	5.7 ± 0.3
χ_M' *vs.* χ_M''/ϖ	O-O	2.5 ± 0.3	24.5 ± 0.7	5.7 ± 0.3	1.62 ± 0.11			
	O-D	1.27 ± 0.16	29.3 ± 0.7			2660 ± 80		
	R-D					2580 ± 50	0.27 ± 11	5.70 ± 0.20
χ_M' *vs.* $\chi_M''\cdot\varpi$	O-O	1.19 ± 0.16	28.2 ± 0.8	3.56 ± 0.16	1.94 ± 0.09			
	O-D	0.65 ± 0.05	32.8 ± 0.5			3583 ± 21		
	R-D					3480 ± 40	0.16 ± 0.05	5.97 ± 0.14
χ_M''/ϖ *vs.* $\chi_M''\cdot\varpi$	O-O	1.48 ± 0.24	27.0 ± 1.0	3.03 ± 0.20	2.37 ± 0.13			
	O-D	1.38 ± 0.19	28.0 ± 0.8			3440 ± 50		
	R-D					3230 ± 40	1.4 ± 0.3	4.99 ± 0.10

[a] O-O, O-D, and R-D stand for Orbach-Orbach, Orbach-Direct, and Raman-Direct combinations, respectively. [b] The values of the preexponential factor (τ_0) and activation energy (E_a) are calculated through the Arrhenius law [$\tau^{-1} = \tau_0^{-1} \exp(-E_a/k_BT)$]. [c] The preexponential coefficient for the Direct mechanism [$\tau^{-1} = AT$]. [d] The preexponential and exponential coefficients for the Raman mechanism [$\tau^{-1} = CT^n$].

Table S12. Selected ac magnetic data for **2** under H_{dc} = 1000 G

Method	Model[a]	τ_{01}[b] × 10^7 (s)	E_{a1}[b] (cm^{-1})	τ_{02}[b] × 10^5 (s)	E_{a2}[b] (cm^{-1})	A[c] (s^{-1} K^{-1})	C[d] (s^{-1} K^{-n})	n[d]
χ_M' *vs.* T	O-O	4.7 ± 1.3	9.4 ± 0.9	7 ± 7	0.3 ± 1.1			
	O-D	0.36 ± 0.04	10.5 ± 0.3			5600 ± 130		
	R-D					4000 ± 400	250 ± 70	4.10 ± 0.21
χ_M' *vs.* ν	O-O	4.0 ± 1.0	15.6 ± 0.9	1.62 ± 0.07	1.68 ± 0.06			
	O-D	3.6 ± 1.2	17.4 ± 1.1			9400 ± 50		
	R-D					9300 ± 60	2.0 ± 1.0	5.7 ± 0.3
χ_M' *vs.* χ_M''/ϖ	O-O	23.2 ± 1.7	9.6 ± 0.4	4.0 ± 0.4	0.41 ± 0.15			
	O-D	10 ± 7	18 ± 3			8610 ± 150		
	R-D					8140 ± 230	3 ± 7	4.6 ± 0.9
χ_M' *vs.* χ_M''·ϖ	O-O	4.1 ± 0.3	16.8 ± 0.4	1.48 ± 0.05	1.79 ± 0.06			
	O-D	3.7 ± 0.4	18.8 ± 0.5			9570 ± 60		
	R-D					9170 ± 140	17 ± 6	4.18 ± 0.17
χ_M''/ϖ *vs.* χ_M''·ϖ	O-O	21.1 ± 1.0	9.3 ± 0.3	3.7 ± 0.3	0.48 ± 0.18			
	O-D	16 ± 4	14.4 ± 1.2			9130 ± 140		
	R-D					8800 ± 4300	40 ± 40	3.4 ± 0.4

[a] O-O, O-D, and R-D stand for Orbach-Orbach, Orbach-Direct, and Raman-Direct combinations, respectively. [b] The values of the preexponential factor (τ_0) and activation energy (E_a) are calculated through the Arrhenius law [$\tau^{-1} = \tau_0^{-1} \exp(-E_a/k_BT)$]. [c] The preexponential coefficient for the Direct mechanism [$\tau^{-1} = AT$]. [d] The preexponential and exponential coefficients for the Raman mechanism [$\tau^{-1} = CT^n$].

Table S13. Selected ac magnetic data for **2** under H_{dc} = 2000 G

Method	Model[a]	τ_{01}[b] × 10^7 (s)	E_{a1}[b] (cm^{-1})	τ_{02}[b] × 10^5 (s)	E_{a2}[b] (cm^{-1})	A[c] (s^{-1} K^{-1})	C[d] (s^{-1} K^{-n})	n[d]
	O-O	3 ± 4	11 ± 6	10 ± 150	0 ± 16			
χ_M' *vs.* T	O-D	2.5 ± 1.0	12.0 ± 1.1			3000 ± 700		
	R-D					700 ± 1500	230 ± 200	4.0 ± 0.6
	O-O	1.2 ± 0.3	20.0 ± 0.8	1.75 ± 0.05	1.49 ± 0.04			
χ_M' *vs.* ν	O-D	0.06 ± 0.06	32 ± 4			9570 ± 70		
	R-D					9560 ± 30	0.0011 ± 0.0023	10.2 ± 1.3
	O-O	14.1 ± 1.3	11.6 ± 0.5	4.3 ± 0.4	0.33 ± 0.16			
χ_M' *vs.* χ_M''/ϖ	O-D	5 ± 3	20 ± 3			7920 ± 200		
	R-D					7800 ± 300	2 ± 4	4.9 ± 1.0
	O-O	1.73 ± 0.12	20.1 ± 0.4	1.96 ± 0.06	1.07 ± 0.05			
χ_M' *vs.* $\chi_M''\cdot\varpi$	O-D	0.39 ± 0.23	30 ± 3			10340 ± 210		
	R-D					10300 ± 300	0.2 ± 0.3	6.5 ± 0.8
	O-O	4.7 ± 0.7	16.2 ± 0.8	2.09 ± 0.17	1.26 ± 0.14			
χ_M''/ϖ *vs.* $\chi_M''\cdot\varpi$	O-D	2.0 ± 0.6	22.7 ± 1.4			9060 ± 120		
	R-D					8890 ± 190	2.4 ± 2.0	5.1 ± 0.4

[a] O-O, O-D, and R-D stand for Orbach-Orbach, Orbach-Direct, and Raman-Direct combinations, respectively. [b] The values of the preexponential factor (τ_0) and activation energy (E_a) are calculated through the Arrhenius law [$\tau^{-1} = \tau_0^{-1} \exp(-E_a/k_BT)$]. [c] The preexponential coefficient for the Direct mechanism [$\tau^{-1} = AT$]. [d] The preexponential and exponential coefficients for the Raman mechanism [$\tau^{-1} = CT^n$].

Table S14. Selected ac magnetic data for **2** under H_{dc} = 3500 G

Method	Model[a]	τ_{01}[b] × 10^7 (s)	E_{a1}[b] (cm^{-1})	τ_{02}[b] × 10^5 (s)	E_{a2}[b] (cm^{-1})	A[c] (s^{-1} K^{-1})	C[d] (s^{-1} K^{-n})	n[d]
χ_M' *vs.* T	O-O	1.9 ± 0.4	12.4 ± 0.5	12.5 ± 0.8	0 ± 0.07			
	O-D	1.2 ± 0.3	14.1 ± 0.6			3830 ± 160		
	R-D					3000 ± 300	36 ± 17	5.3 ± 0.3
χ_M' *vs.* ν	O-O	4.0 ± 0.4	15.9 ± 0.4	1.93 ± 0.04	1.36 ± 0.03			
	O-D	0.3 ± 0.3	27 ± 3			9520 ± 60		
	R-D					9500 ± 80	0.012 ± 0.021	8.7 ± 1.1
χ_M' *vs.* χ_M''/ϖ	O-O	2.7 ± 0.4	20.0 ± 0.7	2.15 ± 0.09	1.37 ± 0.08			
	O-D	0.6 ± 0.4	30 ± 3			8090 ± 120		
	R-D					8040 ± 160	0.08 ± 0.11	6.7 ± 0.7
χ_M' *vs.* $\chi_M''\cdot\varpi$	O-O	0.90 ± 0.05	23.9 ± 0.3	2.27 ± 0.07	0.51 ± 0.05			
	O-D	0.15 ± 0.12	37 ± 5			11000 ± 400		
	R-D					10900 ± 500	0.04 ± 0.08	7.0 ± 1.0
χ_M''/ϖ *vs.* $\chi_M''\cdot\varpi$	O-O	2.9 ± 0.5	29.1 ± 1.0	2.16 ± 0.17	1.00 ± 0.14			
	O-D	0.7 ± 0.5	30 ± 4			9580 ± 230		
	R-D					9500 ± 300	0.2 ± 0.3	6.2 ± 0.9

[a] O-O, O-D, and R-D stand for Orbach-Orbach, Orbach-Direct, and Raman-Direct combinations, respectively. [b] The values of the preexponential factor (τ_0) and activation energy (E_a) are calculated through the Arrhenius law [$\tau^{-1} = \tau_0^{-1} \exp(-E_a/k_BT)$]. [c] The preexponential coefficient for the Direct mechanism [$\tau^{-1} = AT$]. [d] The preexponential and exponential coefficients for the Raman mechanism [$\tau^{-1} = CT^n$].